# Adsorption of phosphate onto lanthanum-doped coal fly ash—Blast furnace cement composite

Asaoka, Satoshi ; Kawakami, Kohei ; Saito, Hiroyuki ; Ichinari, Tsuyoshi ; Nohara, Hideaki ; Oikawa, Takahito

(Citation)
Journal of Hazardous Materials,406:124780

(Issue Date)
2021-03-15

(Resource Type)
journal article

(Version)
Accepted Manuscript



(URL)
https://hdl.handle.net/20.500.14094/90007836

# Adsorption of phosphate onto lanthanum-doped coal fly ash—blast furnace cement composite

Satoshi ASAOKA[a]*, Kohei KAWAKAMI[b], Hiroyuki SAITO[c], Tsuyoshi ICHINARI[c], Hideaki NOHARA[d], Takahito OIKAWA[d]

a Research Center for Inland Seas, Kobe University

5-1-1 Fukaeminami, Higashinada, Kobe, 658-0022 JAPAN

（Present address）Graduate School of Integrated Sciences for Life, Hiroshima University

1-4-4 Kagamiyama, Higashi-Hiroshima, Hiroshima, 739-8528 JAPAN

b Graduate school of Maritime Sciences, Kobe University

5-1-1 Fukaeminami, Higashinada, Kobe, 658-0022 JAPAN

c FujiClean Co., LTD.

33 Yamahana, Yamayashiki, Chiryu, 472-0022 JAPAN)

d The Chugoku Electric Power Co., INC.

3-9-1, Kagamiyama, Higashi-Hiroshima, 739-0046 JAPAN

*Corresponding author:

19 Tel: +81-82-424-7945, E-mail: stasaoka@hiroshima-u.ac.jp

20 Address: Graduate School of Integrated Sciences for Life, Hiroshima University

21 1-1-4 Kagamiyama, Higashi-Hiroshima, Hiroshima, 739-8528 JAPAN

22

23 **Abstract**

24 We develop a high-performance adsorbent for phosphate removal from water or
25 wastewater by impregnating lanthanum (La) on a coal fly ash—blast furnace cement
26 composite (La-FACC). The optimized impregnation percentage of La and calcination
27 conditions of the La-FACC were 1% and 800 ℃ for 2 h, respectively. The adsorption
28 kinetics of phosphate onto the La-FACC was well fit by the intra-particle diffusion model,
29 indicating that film and intra-particle diffusion were the rate-controlling step in the
30 adsorption process of phosphate onto the La-FACC. The pseudo second-order kinetic
31 model could also describe the adsorption kinetics of phosphate. Hence, adsorption of
32 phosphate onto the La-FACC occurred mainly via chemisorption. The Langmuir isotherm
33 was appropriate for describing the phosphate adsorption behavior onto the La-FACC. The
34 monolayer maximum adsorption capacity was 24.9 mg-P $g^{-1}$. The La-FACC showed high
35 adsorption capacity and selectivity for phosphate with a wide range of pH, and with high
36 concentrations of coexisting ions attributed to both formation of inner sphere complexes

and electrostatic interaction. Magnesium ion slightly inhibited the adsorption of phosphate. Hence, the La-FACC developed in this study is a promising adsorbent for water treatment with a wide pH range and high ion strength.

**Key Words**

coal fly ash; lanthanum; phosphate adsorption; recycled materials; waste water treatment

**Highlights**

- Lanthanum-doped adsorbent for phosphate was developed.
- The lanthanum support carrier was mixture of coal fly ash and blast furnace cement.
- The monolayer maximum adsorption capacity of the adsorbent was 24.9 mg-P $g^{-1}$.
- The adsorbent showed high adsorption capacity and selectivity for phosphate
- The adsorbent shown high adsorption capacity with wide pH.

55

56 **Introduction**

57 Phosphorus is an essential substance for living organisms, a component of DNA,
58 RNA, ATP, and phospholipids. Furthermore, phosphorus is necessary for the formation
59 bones and teeth in all vertebrates. Demand for phosphorus has been increasing with the
60 rising demand for food to meet the needs of the growing global population, because
61 phosphate is essential for high crop yields in agriculture (Childers et al., 2011).
62 Agricultural demand over the last 75 years—a result of the Green Revolution—has
63 increased global phosphorus mobilization roughly fourfold (Childers et al., 2011).

64 Currently, agribusiness and plant factories using biotechnology and ICT (information
65 and communication technology) to produce high-value-added plants such as organic
66 vegetables, functional vegetables, and medicinal plants are widespread (Yanata et al.,
67 2015). However, the excessive discharge of phosphate from industrial or domestic
68 wastewater and cultivated fields into water bodies and lakes leads to eutrophication,
69 including the proliferation of harmful algal blooms and formation of hypoxia in coastal
70 marine ecosystems (Conley et al., 2009; Asaoka and Yamamoto, 2011). Secondary
71 effluent from municipal wastewater treatment plants (WWTPs) are considered a main
72 source of such nutrients (Citulski et al., 2009; Gao et al., 2016).

73 Treatments proposed to remove phosphate from wastewater have included biological
74 treatment, chemical precipitation and crystallization (Hiraishi et al., 1998; Wang et al.,
75 2012; Yang et al., 2016; Huang et al., 2017; Lei et al., 2017; Mulder et al., 2018). Most
76 of these technologies are generally available for the removal of high concentration
77 phosphate. In contrast, adsorption is a promising method for removing low concentrations
78 of phosphate in wastewater. Many adsorbents have been developed for phosphate removal,
79 including Fe-Al-Mn ternary oxide, iron oxides, zeolite, hydrotalcite etc. (Hermassi et al.,
80 2016; Abebe et al., 2017; Ajmal et al., 2018; He et al., 2018; Peng et al., 2019; Hsu et al.,
81 2019; Ogata et al., 2019). In particular, lanthanum (La), which is considered
82 environmentally friendly and is relatively abundant in the earth's crust, has a high affinity
83 to phosphate with the formation of the La–phosphate complex (Xie et al, 2014). La
84 doped with suitable substrates has been proven to improve phosphate adsorption
85 efficiency (Zhang et al., 2010; Zhang et al., 2012). Therefore, La has been attracting
86 attention as a material for developing new adsorbents for removal of phosphate from
87 wastewater.

88 In this study, we develop a cost effective La support carrier by mixing coal fly ash
89 from an electric power plant with blast furnace cement (Asaoka et al., 2012; Asaoka et
90 al., 2014; Asaoka et al., 2017). When coal fly ash is mixed with cement, the silicon oxide

91 and aluminum oxide contained in the coal fly ash react with the calcium hydroxide in the
92 blast furnace cement in what is called the pozzolanic reaction (Shi and Day, 2000a,
93 2000b). This reaction increases the specific surface area. Therefore, a coal fly ash—blast
94 furnace cement composite (FACC) prepared by the pozzolanic reaction with high specific
95 surface area (11.4 $m^2$ $g^{-1}$; Asaoka et al., 2017) is an advantageous support carrier for La
96 doping. Annual global generation of fly ash is estimated to be approximately 750 million
97 tons (Yao et al., 2015). Therefore, new applications utilizing byproducts from coal-fired
98 power plants are expected to contribute to waste reduction and promote recycling within
99 society.

100 The purposes of this study are to: (1) optimize the preparation conditions of an
101 adsorbent for phosphate, the La-doped coal fly ash—blast furnace cement composite (La-
102 FACC), and (2) verify the phosphate adsorption performance of the La-FACC.

103

104 **Experimental**

105 **2.1 Preparing the La-FACC**

106 The La support carrier was prepared by mixing with coal fly ash (Chugoku Electric
107 Power Co., Inc., Japan) and blast furnace cement (Class B: Nippon Steel Blast Furnace
108 Slag Cement Co., Ltd, Japan). The mixing ratio of coal fly ash and blast furnace cement

was 7:3 by mass, which was found to be the most effective for increasing the specific surface area of the composite (Asaoka et al., 2017). Then, the mixture was sprayed with 12.5% pure water to the total weight of the mixed composite. The composite was then granulated to approximately 5-mm diameter using a rotary pan granulator (PZ-01R: AZ ONE, Japan). Pure water was sprayed so as to wet the surface of the granulated composite every day for the first week. The granulated composite was then air-dried for at least 3 months in a laboratory at 25 ℃ to complete the pozzolanic reaction between the coal fly ash and blast furnace cement. Finally, the granulated composite was sieved to a diameter of 1.00–3.35 mm.

La was impregnated into the granulated composite by the incipient wetness impregnation method. The granulated composite was immersed in an aqueous solution containing an La precursor, lanthanum chloride hepta-hydrate (Wako Special Grade, FUJIFILM Wako Chemicals, Japan) for 1 day at 25 ℃. After impregnation, the lanthanum chloride hepta-hydrate solution was evaporated to dryness at 105 ℃ in a dry oven. The La-doped composite was calcined at 800 ℃ for 2 h in air using an electric furnace (HPM-0N, AZ ONE, Japan), and then allowed to cool naturally in the furnace.

The amount of La doped on the granulated composite was controlled by dissolving different amounts of lanthanum chloride hepta-hydrate into pure water. The impregnation

127 percentage of La in the final La-FACC product was verified by determining the
128 concentration of La using a wavelength dispersive type X-ray fluorescence analyzer
129 (Supermini; Rigaku, Japan) with fundamental parameter mode. The chemical
130 composition of the optimized La-FACC is presented in **Table 1**.

131 The zeta potential of the powdered FACC and La-FACC in 10 mmol $L^{-1}$ NaCl solution
132 was analyzed at different pH ranging from 3 to 10 using a zeta-potential & particle size
133 analyzer (ELSZ-2000; Otsuka Electronics, Japan).

134

135 **2.2 Optimization of calcination conditions of the La-FACC**

136 La-FACC calcination temperature and time varied in the range of 600–1000 ºC and
137 0.5–8 h, respectively. Batch experiments were carried out to investigate the effects of
138 calcination conditions on the adsorption of phosphate onto La-FACC. Five g $L^{-1}$ samples
139 of La-FACC were placed in Erlenmeyer flasks with 100 mg-P $L^{-1}$ solution prepared by
140 dissolving sodium dihydrogen phosphate dihydrate (Guaranteed Reagent, FUJIFILM
141 Wako Chemicals, Japan) in ultrapure water. The Erlenmeyer flasks were closed with
142 silicosen plugs (Shin-Etsu Polymer, Japan), and then agitated at 100 rpm at 25 ºC in a
143 constant-temperature oven. After reaching equilibrium (168 h), the phosphate solution
144 was filtered with a 0.45-μm pore syringe filter (SLHN033NB; Merck, Germany).

145 The phosphate concentration in the filtrate was analyzed by molybdenum blue
146 absorption photometry (Motomizu et al., 1983) using a flow injection analyzer (FIA-$PO_4$;
147 Kyoritsu Chemical-Check Lab, Japan). The initial and final pH of the phosphate solution
148 was measured with a pH meter (LAQUA twin B-711; Horiba, Japan). We also conducted
149 batch experiments without the La-FACC using the same procedure as a control. These
150 batch experiments were conducted in triplicate. The phosphate adsorbed per gram of La-
151 FACC was calculated using Eq. (1).

152 $$Q_e = \frac{(C - C_e)V}{W} \qquad (1)$$

153 where $C$ and $C_e$ represent the concentrations of phosphate of the control and the La-FACC
154 applied solution (mg-P $L^{-1}$) at equilibrium, respectively, $Q_e$ (mg-P $g^{-1}$) indicates the
155 amount of phosphate adsorbed per unit weight (g) of the La-FACC, $W$ shows the mass of
156 the applied La-FACC (g), and $V$ is the volume of the phosphate solution (L).

157

158 **2.3 Optimization of impregnation percentage of La in the La-FACC**

159 The impregnation percentage of La in the La-FACC was varied within the range of
160 0.1–4%. The batch experiments investigated the effects of impregnation percentage of La
161 in the La-FACC on adsorption of phosphate following the procedure described in **2.2**.

162 The load to collapse the La-FACC particles was easily measured by a digital force

gauge (DST-500N; IMADA, Japan) attached with a cone-type attachment (S-3, IMADA, Japan).

### 2.4 Adsorption kinetics of phosphate onto the La-FACC

The 1 g $L^{-1}$ of La-FACC samples were placed in Erlenmeyer flasks with 10, 25 and 100 mg-P $L^{-1}$ solution. The batch experiments were carried out using the procedure described in **2.2**, and then aliquots of the phosphate solution were taken at regular intervals to determine residual phosphate in the solution. The adsorption kinetics of phosphate onto the La-FACC was fit by the three well-known models: pseudo first-order model, pseudo second-order model, and intra-particle diffusion model. The equations of these models are expressed as Eqs. (2)-(4), respectively.

$$\log(Q_e - Q_t) = logQ_e + \frac{k_1}{2.303}t \quad (2)$$

$$\frac{t}{Q_t} = \frac{1}{k_2 Q_e^2} + \frac{1}{Q_e}t \quad (3)$$

$$Q_t = k_i t^{\frac{1}{2}} \quad (4)$$

where $t$ represents contact time (h), $Q_e$, and $Q_t$ (mg-P $g^{-1}$) indicate the amount of phosphate adsorbed per unit weight (g) of the La-FACC at equilibrium and the amount of phosphate adsorbed per unit weight (g) of La-FACC at time t (h), respectively, and $k_1$ ($h^{-1}$) , $k_2$ (g $mg^{-1}$ $h^{-1}$) and $k_i$ (mg $g^{-1}$ $h^{-1/2}$) are the rate constants for the pseudo first-order, second-order,

and intra-particle diffusion models, respectively.

The adequacy of kinetic models was verified by calculating percentage deviation (D%) between observed and calculated amounts of phosphate adsorbed onto the La-FACC at equilibrium using Eq. 5 (Rehman, et al., 2013).

$$D(\%) = \frac{(Q_{e,obs} - Q_{e,cal})}{Q_{e,cal}} \cdot 100 \quad (5)$$

where, $Q_{e,\,obs}$ (mg-P $g^{-1}$) and $Q_{e,\,cal}$ (mg-P $g^{-1}$) indicate the observed or calculated amount of phosphate, respectively, adsorbed per unit weight (g) of the La-FACC at equilibrium.

**2.5 Adsorption isotherm of phosphate onto the La-FACC**

The 5 g $L^{-1}$ of La-FACC samples were placed in Erlenmeyer flasks with 10–200 mg-P $L^{-1}$ solution. Batch experiments were carried using the procedure described in **2.2.** The adsorption behavior of phosphate onto the La-FACC was expressed as Langmuir (Eq. 6), Freundlich (Eq. 7) and Dubinin–Radushkevich (Eq. 8: Dubinin and Radushkevich, 1947) isotherms.

$$\frac{C_e}{Q_e} = \frac{1}{ab} + \frac{C_e}{a} \quad (6)$$

$$\log Q_e = logF + \frac{1}{n} logC_e \quad (7)$$

$$q_e = q_m e^{-K_d \varepsilon^2} \quad (8)$$

where $C_e$ (mg-P $L^{-1}$) represents the equilibrium phosphate concentration, $a$ (mg-P $g^{-1}$) indicates the maximum adsorption capacity, $b$ (L $mg^{-1}$) represents the adsorption equilibrium constant, and $F$ and $n$ are the Freundlich constants, which show the amount of phosphate adsorbed for unit equilibrium concentration and the intensity of the adsorption process, respectively. $Q_e$ (mg-P $g^{-1}$) indicates the amount of phosphate adsorbed per unit weight (g) of the La-FACC at equilibrium.

Dimensionless constant separation factor ($R_L$) of the Langmuir isotherm was calculated using Eq. 9 (Huang et al., 2014).

$$R_L = \frac{1}{1 + bC_i} \quad (9)$$

where $b$ indicates the adsorption equilibrium constant (L $mg^{-1}$) obtained by the Langmuir isotherm, and $C_i$ is the initial concentration of phosphate (mg-P $L^{-1}$).

In the case of Dubinin–Radushkevich isotherms (Eq. 8), $q_e$ (mol $g^{-1}$) represents the molar of the phosphate adsorbed per unit weight (g) of La-FACC at the equilibrium, and $q_m$ (mol $g^{-1}$) the theoretical isotherm saturation capacity of the La-FACC. $K_d$ is the Dubinin–Radushkevich isotherm constant ($mol^2$ $kJ^{-2}$), and $\varepsilon$ the Dubinin–Radushkevich

217 isotherm constant calculated following Eq. 10 (Hasany and Chaudhary, 1996;
218 Benhammou et al., 2005; Akar et al., 2013).

219 $$\varepsilon = \mathrm{RTln}\left(1 + \frac{1}{C_{me}}\right) \quad (10)$$

220 where R, represents the gas constant ($8.314 \cdot 10^{-3}$ kJ $mol^{-1}$ $K^{-1}$), T is absolute temperature
221 (K), and and $C_{me}$ is the phosphate equilibrium concentration (mol $L^{-1}$).

222 The root mean squared error (RMSE) between estimated the amount of phosphate
223 adsorbed on the La-FACC obtained by the three isotherms ($Q_{e,\ cal}$) and the those of
224 observed values ($Q_{e,\ obs}$) was calculated by Eq.11.

225 $$\mathrm{RMSE} = \sqrt{\frac{\sum_{i=1}^{n}\left(Q_{e,obs} - Q_{e,cal}\right)^2}{n}} \quad \cdot\ \cdot\ \cdot (11)$$

226

227 **2.6 Effect of solution pH on adsorption of phosphate onto the La-FACC**

228 We investigated the effect of solution pH on phosphate adsorption onto the La-FACC
229 in the same manner with batch experiments as described in **2.2**, except that the initial
230 phosphate concentration was 200 mg-P $L^{-1}$. The solution pH was kept within the desired
231 range of 4–10 by addition of 0.1 mol $L^{-1}$ HCl or NaOH to the solution.

232

233 **2.7 Effect of coexisting ions on adsorption of phosphate onto the La-FACC**

234 The effect of 100 mg $L^{-1}$ of coexisting ions on phosphate adsorption onto the La-

235 FACC was examined with batch experiments, as described in **2.2**. The solutions of
236 coexisting ions such as $Na^+$, $K^+$, $Ca^{2+}$, $Mg^{2+}$, $Cl^-$, $NO_2^-$, $NO_3^-$ and $SO_4^{2-}$ used in this study
237 were prepared from their respective salts sodium chloride, potassium chloride, calcium
238 chloride, magnesium chloride hexahydrate, potassium nitrite, potassium nitrate and
239 potassium sulfate, respectively.
240

241 **3. Results and discussion**

242 **3.1 Optimization of calcination conditions of the La-FACC**

243 Calcination conditions were optimized to prepare the La-FACC. The effect of
244 calcination temperature on La-FACC phosphate adsorption was investigated, as shown in
245 **Fig. 1**. The pH of the solution varied in the range of 7.8–8.2 at equilibrium. The phosphate
246 adsorbed per g of La-FACC (impregnation percentage of La: 4%; calcination time: 2 h)
247 showed no statistical difference in the calcination temperature range of 600–800 ºC.
248 However, in La-FACC calcined at 600 and 700 ºC, white La phosphate precipitation
249 exfoliated from the La-FACC was observed in the liquid phase after the batch experiments
250 (**Fig. S1**). In contrast, the exfoliation of La phosphate from the La-FACC was not
251 observed at calcination temperatures at 800 ºC.
252 On the other hand, at temperatures between 900 and 1000 ºC, phosphate adsorption

capacity of the La-FACC decreased compared to that between 600–800 ºC (statistical significance level: p-value <0.01). This decrease in phosphate adsorption capacity was due to the reduced number of adsorption sites for phosphate. Xie et al. (2014) reported that phosphate adsorption on La is performed by the formation of an inner-sphere complex ($\equiv LaO\text{-}PO_3^{2-}$). Because the surface pH of FACC was 11.7 (Asaoka et al., 2017), the zeta potential of the FACC was negative (**Fig. S2**). Hence, it is considered $La^{3+}$ adsorbed on the surface of negatively charged FACC through the incipient wetness impregnation. When the calcination temperature exceeds 400 ℃, LaCl is transformed into LaOCl and bonds to the fly ash—blast furnace cement composite. In turn, LaOCl is transformed to $La_2O_3$ above 800 ℃(Kim et al., 2000). Therefore, we consider that most phosphate adsorption sites in the La-FACC calcined at 900 and 1000 ℃ were transformed to inactive $La_2O_3$ from active LaOCl. Hence, the calcination temperature was optimized to 800 ℃ to obtain high adsorption capacity without exfoliating La phosphate from the La-FACC.

The calcination time was also investigated in the range of 0.5–8 h. When the calcination time was 0.5–4 h, the phosphate adsorption capacity of La-FACC did not show a statistical difference. However, the phosphate adsorption capacity of La-FACC calcined for 8 h decreased slightly (3.5-6.0%) compared to that at 0.5–4 h ($p < 0.05$). Therefore,

271 calcination time was optimized to 2 h to allow some margin.

272

273 **3.2 Optimization of impregnation percentage of La in the La-FACC**

274 The impregnation percentage of La on the La-FACC was investigated in the range of
275 0.1–4%. The solution pH was in the range of 7.9–8.3 at equilibrium. When the
276 impregnation percentage of La on the La-FACC was between 0.1–1%, the phosphate
277 adsorption capacity of the La-FACCs ranged from 19.9–20.6 mg $g^{-1}$ without a statistical
278 difference (**Fig. 2**). However, when the percentage of La exceeded 1%, the phosphate
279 adsorbed per g of La-FACCs decreased ($p < 0.01$). The surface pH of the La-FACC can
280 affect the phosphate adsorbed per g. Moreover, the species of phosphate ion differs at
281 different pH, as shown by the following equations (Huang et al., 2014).

282 $H_3PO_4 \Leftrightarrow H_2PO_4^- + H^+ \quad pK_{a1}=2.15$

283 $H_2PO_4^- \Leftrightarrow HPO_4^{2-} + H^+ \quad pK_{a2}=7.20$

284 $HPO_4^{2-} \Leftrightarrow PO_4^{3-} + H^+ \quad pK_{a3}=12.33$

285 We calculated the species of 100 mg-P $L^{-1}$ of phosphate at different pH using the
286 chemical equilibrium model software, Visual MINTEQ ver.3.0 (**Fig. S3**). For a
287 impregnation percentage of La between 0.1–1%, the surface pH of the La-FACC ranged
288 from 9.5–10.2 **(Fig. 2**). Within this pH range (9.5-10.3), $HPO_4^{2-}$ was the major species of

289 phosphate, accounting for 98.9–99.4% of all phosphate. In contrast, with impregnation
290 percentage of La of 2% and 4% the surface pH was 7.4 and 6.9 (**Fig. 2**); the phosphate
291 species were 33.4% $H_2PO_4^-$ and 66.6% $HPO_4^{2-}$ at pH 7.4, and 62.1% and 37.9% at pH 6.9
292 (**Fig. S3**). Therefore, the electrostatic interaction between the 2% or 4% La-doped La-
293 FACC and phosphate was lower than that of 0.1–1% La-doped La-FACC. Hence, we
294 considered the adsorption capacity of 2 or 4% La-doped La-FACC to be decreased.
295 The load to collapse the La-FACC particles were 2.8, 1.9, 4.1, 4.5 and 5.0 N for the
296 La-FACC with 0.1, 0.5, 1, 2 and 4%, respectively, of the La impregnated La-FACC. When
297 the load exceeded 3 N, the crushing strength of the La-FACC particle was sufficient for
298 stirring or filling in a wastewater treatment column. Therefore, the optimum impregnated
299 percentage of La on the La-FACC was 1%, taking into account both the phosphate
300 adsorption capacity and crushing strength.
301
302 **3.3 Adsorption kinetics of phosphate onto the optimized La-FACC**
303 In the case of initial concentration of 100 mg-P $L^{-1}$, the adsorption of phosphate onto the
304 La-FACC reached 90% of equilibrium adsorption within 72 h and at equilibrium within
305 168 h. Adsorption kinetics for phosphate onto the optimized La-FACCs were fit by three
306 kinetic models: the pseudo first-order model (Eq. 2), pseudo second-order model (Eq. 3)

307 and intra-particle diffusion model (Eq. 4). The results of parameter fitting using the three
308 kinetic models are shown in **Table 2**. In the case of 10 and 25 mg-P $L^{-1}$, the intra-particle
309 diffusion model, which indicates film diffusion, showed linearity (**Fig. 3**). The straight
310 lines fit by the intra-particle diffusion model did not pass through the origin, implying the
311 coexistence of both film and intra-particle diffusion mechanisms (Lalley, et al., 2016;
312 Ajmal et al., 2018). In the case of 100 mg-P $L^{-1}$, the adsorption kinetics could be fit by
313 the intra-particle diffusion model for the first 48 h (6.9 $h^{-1/2}$). Therefore, it is considered
314 that film and intra-particle diffusion are the rate-controlling step in the adsorption process
315 of phosphate for the first 48 h. Furthermore, the pseudo second-order kinetic model could
316 describe the adsorption kinetics of phosphate (**Fig. 4**). The coefficient of determinations
317 for the pseudo second-order kinetic model ($R^2$=0.979-0.998) were higher than those of
318 the pseudo first-order model ($R^2$=0.751-0.965). The deviation in the amount of phosphate
319 adsorbed onto the La-FACC at equilibrium ($Q_e$) fit by the pseudo second-order kinetic
320 model was much lower compared to that of the pseudo first-order model (**Table 2**). These
321 results indicate adsorption of phosphate onto the La-FACC occurs mainly via
322 chemisorption (Ho and McKay, 1999).
323

324 **3.4 Adsorption isotherm of phosphate onto the La-FACC**

325 The adsorption behavior of phosphate onto optimized La-FACC has been investigated
326 by Langmuir (Eq. 6), Freundlich (Eq. 7) and Dubinin–Radushkevich (Eq. 8) adsorption
327 isotherms (**Fig. 5**). The coefficient of determination, p-value, and RMSE between
328 observed and calculated amounts of phosphate adsorbed on the La-FACC are shown in
329 **Table 3**. The Langmuir isotherm ($R^2$=0.992, RMSE=2.80) fit well with observed values
330 compared to the Freundlich isotherm ($R^2$=0.657, RMSE=5.28) and Dubinin–
331 Radushkevich isotherm ($R^2$=0.703, RMSE=11.9). The Langmuir isotherm is therefore
332 appropriate for describing the phosphate adsorption behavior of the La-FACC. Hence, the
333 adsorption behavior of phosphate onto the La-FACC was a monolayer adsorption, which
334 is in good agreement with previous findings on La-modified adsorbents, such as La-
335 modified bentonite (Haghseresht et al., 2009), La hydroxide-doped activated carbon fiber
336 (Zhang et al., 2012) and La-loaded biochar (Wang et al., 2016). The adsorption
337 equilibrium constant, $b$ (L $mg^{-1}$) and maximum monolayer adsorption capacity $a$ (mg-P
338 $g^{-1}$) obtained by the Langmuir isotherm were 0.212 L $mg^{-1}$ and 24.9 mg-P $g^{-1}$, respectively.
339 The estimated maximum monolayer adsorption capacity was in good agreement with
340 observed values (23.6 mg-P $g^{-1}$). The observed lanthanum utilization efficiency (La/P
341 molar ratio) was 0.090.
342 The dimensionless separation factor ($R_L$) calculated by Eq. 9 indicates adsorption

characteristics as follows (Memon et al., 2008; Balouch et al., 2013): $R_L = 0$: irreversible isotherm, $0 < R_L < 1$: favorable isotherm, $R_L = 1$: linear isotherm, $R_L > 1$: unfavorable isotherm. The calculated $R_L$ values of the La-FACC were between (0.0230–0.321), indicating highly favorable sorption of phosphate onto the La-FACC.

### 3.5 Effect of solution pH on adsorption of phosphate onto the La-FACC

The effect of final pH at equilibrium on the maximum adsorption capacity of phosphate onto the La-FACC was investigated at the final pH range of 4.1–9.6 (**Fig. 6**). The maximum adsorption capacity rose with increased final pH from 5.3–8.3, reached a plateau within a final pH range from 8.3–8.9, then decreased at a final pH of 9.6.

The point of zero charge ($pH_{pzc}$) of the La-FACC was pH 7.1 and 3.0 (**Fig. 7**). When the pH value is 3.0 to 7.1, phosphate adsorption mainly proceeded by a ligand exchange process, giving rise to the formation of inner-sphere complex (Zhang et al., 2012; Xie et al., 2014). This ligand exchange process at such high pH was also reported in a previous study (Elzinga and Sparks, 2007). Additionally, the surface hydroxyl groups of can be protonated. The surface positive charge can interact with the anionic phosphate by electrostatic forces (Zhang et al., 2012). Again, the acid dissociation constants of phosphate are $pK_{a1}$=2.15, $pK_{a2}$=7.20 and $pK_{a3}$=12.33 (Huang et al., 2014). Therefore, the

361 dominant phosphate ion species transformed into divalent $HPO_4^{2-}$ from monovalent
362 $H_2PO_4^-$ with the increase of final pH from 4.1 to 8.9 (**Fig. S3**), which allowed phosphate
363 to strongly adsorb onto the La-FACC due to the electrostatic interaction with its
364 increasing divalent negative charge. When the pH exceeds the $pH_{pzc}$ (pH7.1), the
365 predominant species are $HPO_4^{2-}$. Simultaneously, the laudanum on the La-FACC is
366 negatively charged ($LaO^-$). The strong electrostatic repulsion between $LaO^-$ and $HPO_4^{2-}$
367 prevents phosphate from approaching to the surface of the La-FACC. Therefore, the
368 ligands exchange become weaker. In contrast, the Lewis acid–base interaction would be
369 strengthened (Zhang et al., 2012). Previous studies reported the decrease of adsorption
370 capacity of phosphate onto some La-doped adsorbents above pH 6–8 (Tian et al., 2009:
371 Zhang et al., 2010; Huang et al, 2014). In contrast, the La-FACC proposed in this study
372 maintained high adsorption capacity at pH above 8, which is advantageous for water
373 treatment with a wide pH range.
374
375 **3.6 Effect of coexisting ions on adsorption of phosphate onto La-FACC**
376 The effect of coexisting ions on adsorption of phosphate onto the La-FACC were
377 evaluated in the presence of $Na^+$, $K^+$, $Ca^{2+}$, $Mg^{2+}$, $Cl^-$, $NO_2^-$, $NO_3^-$ and $SO_4^{2-}$. **Fig. 8** shows
378 the relative removal percentage of phosphate with each coexisting ion against that of the

379 removal percentage of phosphate without them. Inhibition of phosphate adsorption was
380 not observed in the presence of $Na^+$, $K^+$, $Ca^{2+}$ and $SO_4^{2-}$. The presence of $Cl^-$, $NO_3^-$ and
381 $NO_2^-$ decreased the removal percentage of phosphate onto the La-FACC due to the
382 competition between the anions and phosphate for adsorption sites. However, the
383 decrease of removal percentage compared to without coexisting ions was only in the range
384 of 6.3–11.8%, indicating that the La-FACC had a high selectivity for adsorption of
385 phosphate in the presence of anions. When $Mg^{2+}$ was in the phosphate solution, the
386 removal percentage of phosphate was 19.3% lower than that without coexisting ions. The
387 dissolved species of phosphate with $Mg^{2+}$ at pH 8 using a chemical equilibrium model
388 software, Visual MINTEQ ver.3.0., showed the main dissolved species were $HPO_4^{2-}$
389 (55.4%) and $MgHPO_4$ (38.3%), indicating a decrease of $HPO_4^{2-}$ due to formation of
390 $MgHPO_4$, which is likely to inhibit the formation of inner-sphere complex of phosphate.
391 Overall, it is can be said that the La-FACC has high selectivity for phosphate adsorption
392 and is advantageous for water treatment with high ion strength.
393
394 **Conclusions**
395 We developed a high-performance adsorbent, lanthanum-doped coal fly ash—blast
396 furnace cement composite (La-FACC), to remove phosphate from water; the mixture was

397 prepared with 70% coal fly ash and 30% blast furnace cement. The optimized
398 impregnation percentage of La and calcination conditions were 1% and 800 ºC for 2 h,
399 respectively. The maximum adsorption capacity was 24.9 mg-P $g^{-1}$. The La-FACC
400 showed high adsorption capacity for phosphate with a wide pH range. Magnesium ions
401 slightly inhibited the adsorption of phosphate. Hence, the La-FACC developed in this
402 study is a promising adsorbent for water treatment with wide pH range and high ion
403 strength.
404
405 **Acknowledgments**
406 This study was partially supported by the A-STEP program in 2018 (VP30118066263)
407 from Japan Science and Technology Agency.
408
409 **References**
410 Abebe, B., Taddesse, A. M., Kebede, T., Teju, E., Diaz, I., 2017. Fe-Al-Mn ternary oxide
411 nanosorbent: Synthesis, characterization and phosphate sorption property, Journal of
412 Environmental Chemical Engineering, 5(2), 1330-1340. DOI:
413 10.1016/j.jece.2017.02.026
414 Akar, E., Altinişik, A., Seki, Y., 2013. Using of activated carbon produced from spent tea

415 leaves for the removal of malachite green from aqueous solution, Ecological
416 Engineering, 52, 19-27. DOI: 10.1016/j.ecoleng.2012.12.032
417 Ajmal, Z., Muhmood, A., Usman, M., Kizito, S., Lu, J., Dong, R., Wu, S., 2018.
418 Phosphate removal from aqueous solution using iron oxides: adsorption, desorption
419 and regeneration characteristics, Journal of Colloid and Interface Science, 528, 145-
420 155. DOI: 10.1016/j.jcis.2018.05.084
421 Asaoka, S., Yamamoto, T., 2011. Phosphorus mass balance in a highly eutrophic semi-
422 enclosed inlet near a big metropolis: A small inlet can contribute towards particulate
423 organic matter production, Marine Pollution Bulletin, 63(5-12), 237-242. DOI:
424 10.1016/j.marpolbul.2011.02.028
425 Asaoka, S., Hayakawa, S., Kim, K. H., Takeda, K., Katayama, M., Yamamoto, T., 2012.
426 Combined adsorption and oxidation mechanisms of hydrogen sulfide on granulated
427 coal ash, Journal of Colloid and Interface science, 377(1), 284-290. DOI:
428 10.1016/j.jcis.2012.03.023
429 Asaoka, S., Okamura, H., Akita, Y., Nakano, K., Nakamoto, K., Hino, K., Saito, T.,
430 Hayakawa, S., Katayama, M.,Inada, Y., 2014. Regeneration of manganese oxide as
431 adsorption sites for hydrogen sulfide on granulated coal ash, Chemical Engineering
432 Journal, 254, 531-537.DOI: 10.1016/j.cej.2014.06.005

433 Asaoka, S., Okamura, H., Kim, K., Hatanaka, Y., Nakamoto, K., Hino, K., Oikawa, T.,
434 Hayakawa, S., Okuda, T., 2017. Optimum reaction ratio of coal fly ash to blast furnace
435 cement for effective removal of hydrogen sulfide, Chemosphere, 168, 384-389. DOI:
436 10.1016/j.chemosphere.2016.10.070
437 Balouch, A., Kolachi, M., Talpur, F. N., Khan, H., Bhanger, M. I., 2013. Sorption kinetics,
438 isotherm and thermodynamic modeling of defluoridation of ground water using
439 natural adsorbents, American Journal of Analytical Chemistry 4(5), DOI:
440 10.4236/ajac.2013.45028
441 Benhammou, A., Yaacoubi, A., Nibou, L., Tanouti, B., 2005. Adsorption of metal ions
442 onto Moroccan stevensite: kinetic and isotherm studies, Journal of Colloid and
443 Interface Science, 282(2), 320-326. DOI: 10.1016/j.jcis.2004.08.168
444 Childers, D. L., Corman, J., Edwards, M., Elser, J. J. , 2011. Sustainability challenges of
445 phosphorus and food: solutions from closing the human phosphorus cycle,
446 BioScience, 61(2), 117-124. DOI: 10.1525/bio.2011.61.2.6
447 Citulski, J., Farahbakhsh, K., Kent, F., 2009. Optimization of phosphorus removal in
448 secondary effluent using immersed ultrafiltration membranes with in-line coagulant
449 pretreatment d implications for advanced water treatment and reuse applications,
450 Canadian Journal of Civil Engineering, 36(7), 1272-1283. DOI: 10.1139/L09-062.

Conley, D. J., Paerl, H. W., Howarth, R. W., Boesch, D. F., Seitzinger, S. P., Havens, K. E., Lancelot, C., Likens, G. E., 2009. Controlling eutrophication: nitrogen and phosphorus, Science 323(5917), 1014-1015. DOI: 10.1126/science.1167755

Dubinin, M.M., Radushkevich, L.V., 1947. The equation of the characteristic curve of activated charcoal, Proc. Acad. Sci. USSR, Phys. Chem. Sect. 55, 331–333.

Elzinga, E. J., Sparks, D. L., 2007. Phosphate adsorption onto hematite: An in situ ATR-FTIR investigation of the effects of pH and loading level on the mode of phosphate surface complexation, Journal of Colloid and Interface Science, 308(1), 53-70. DOI: 10.1016/j.jcis.2006.12.061

Gao, F., Li, C., Yang, Z.-H., Zeng, G.-M., Mu, J., Liu, M., Cui, W., 2016. Removal of nutrients, organic matter, and metal from domestic secondary effluent through microalgae cultivation in a membrane photobioreactor, Journal of Chemical Technology & Biotechnology. 91(10), 2713-2719. DOI: 10.1002/jctb.4879.

Haghseresht, F., Wang, S., Do, D. D., 2009. A novel lanthanum-modified bentonite, Phoslock, for phosphate removal from wastewaters, Applied Clay Science, 46(4), 369-375. DOI: 10.1016/j.clay.2009.09.009

Hasany, S. M., Chaudhary, M. H., 1996. Sorption potential of Haro river sand for the removal of antimony from acidic aqueous solution, Applied Radiation and Isotopes,

469 47(4), 467-471. DOI: 10.1016/0969-8043(95)00310-X
470 He, Y., Lin, H., Dong, Y., Li, B., Wang, L., Chu, S., Luo, M., Liu, J., 2018. Zeolite
471 supported Fe/Ni bimetallic nanoparticles for simultaneous removal of nitrate and
472 phosphate: synergistic effect and mechanism, Chemical Engineering Journal, 347,
473 669-681. DOI: 10.1016/j.cej.2018.04.088
474 Hermassi, M., Valderrama, C., Moreno, N., Font, O., Querol, X., Batis, N., Cortina, J. L. ,
475 2016. Powdered Ca‐activated zeolite for phosphate removal from treated waste‐
476 water, Journal of Chemical Technology & Biotechnology, 91(7), 1962-1971. DOI:
477 10.1002/jctb.4867
478 Hiraishi, A., Ueda, Y., Ishihara, J., 1998. Quinone profiling of bacterial communities in
479 natural and synthetic sewage activated sludge for enhanced phosphate removal,
480 Applied and Environmental Microbiology., 64(3), 992-998. DOI:
481 10.1128/AEM.64.3.992-998.1998
482 Ho, Y. S., McKay, G. , 1999. Pseudo-second order model for sorption processes, Process
483 Biochemistry, 34(5), 451-465. DOI: 10.1016/S0032-9592(98)00112-5
484 Hsu, L. C., Tzou, Y. M., Chiang, P. N., Fu, W. M., Wang, M. K., Teah, H. Y., Liu, Y. T.,
485 2019. Adsorption mechanisms of chromate and phosphate on hydrotalcite: A
486 combination of macroscopic and spectroscopic studies, Environmental Pollution, 247,

180-187. DOI: 10.1016/j.envpol.2019.01.012

Huang, W. Y., Li, D., Liu, Z. Q., Tao, Q., Zhu, Y., Yang, J., & Zhang, Y. M., 2014. Kinetics, isotherm, thermodynamic, and adsorption mechanism studies of $La(OH)_3$-modified exfoliated vermiculites as highly efficient phosphate adsorbents, Chemical Engineering Journal, 236, 191-201. DOI: 10.1016/j.cej.2013.09.077

Huang, H., Liu, J., Zhang, P., Zhang, D., Gao, F., 2017. Investigation on the simultaneous removal of fluoride, ammonia nitrogen and phosphate from semiconductor wastewater using chemical precipitation, Chemical Engineering Journal, 307, 696-706. DOI: 10.1016/j.cej.2016.08.134

Kim, D. H., Yoon, J. Y., Park, H. C., Kim, K. H., 2000. $CO_2$-sensing characteristics of $SnO_2$ thick film by coating lanthanum oxide, Sensors and Actuators B: chemical, 62(1), 61-66. DOI: 10.1016/S0925-4005(99)00305-6

Lalley, J., Han, C., Li, X., Dionysiou, D. D., Nadagouda, M. N., 2016. Phosphate adsorption using modified iron oxide-based sorbents in lake water: kinetics, equilibrium, and column tests, Chemical Engineering Journal, 284, 1386-1396. DOI: 10.1016/j.cej.2015.08.114

Lei, Y., Song, B., van der Weijden, R. D., Saakes, M., Buisman, C. J. N., 2017. Electrochemical induced calcium phosphate precipitation: importance of local pH,

505 Environmental Science & Technology, 51(19), 11156-11164. DOI:
506 10.1021/acs.est.7b03909
507 Memon, J. R., Memon, S. Q., Bhanger, M. I., Memon, G. Z., El-Turki, A., & Allen, G. C.,
508 2008. Characterization of banana peel by scanning electron microscopy and FT-IR
509 spectroscopy and its use for cadmium removal, Colloids and Surfaces B:
510 Biointerfaces, 66(2), 260-265. DOI: 10.1016/j.colsurfb.2008.07.001
511 Motomizu, S., Wakimoto, T., Tôei, Y., 1983. Determination of trace amounts of phosphate
512 in river water by flow-injection analysis, Talanta, 30(5), 333-338. DOI:
513 10.1016/0039-9140(83)80076-9
514 Mulder, M., Appeldoorn, K., Weij, P., Van Kempen, R., 2018. Full scale optimisation of
515 sludge dewatering and phosphate removal at Harnaschpolder wwtp (The Hague, NL),
516 Water Practice & Technology, 13(1), 21-29. DOI: 10.2166/wpt.2018.008
517 Ogata, F., Nagai, N., Kishida, M., Nakamura, T., Kawasaki, N., 2019. Interaction between
518 phosphate ions and Fe-Mg type hydrotalcite for purification of wastewater, Journal of
519 Environmental Chemical Engineering, 7(1), 102897. DOI:
520 10.1016/j.jece.2019.102897
521 Peng, Y., Sun, Y., Sun, R., Zhou, Y., Tsang, D. C. W., Chen, Q., 2019. Optimizing the
522 synthesis of Fe/Al (Hydr) oxides-Biochars to maximize phosphate removal via

523 response surface model, Journal of Cleaner Production, 237, 117770. DOI:
524 10.1016/j.jclepro.2019.117770
525 Rehman, M. S. U., Munir, M., Ashfaq, M., Rashid, N., Nazar, M. F., Danish, M., Han, J.
526 I., 2013. Adsorption of Brilliant Green dye from aqueous solution onto red clay,
527 Chemical Engineering Journal, 228, 54-62. DOI: 10.1016/j.cej.2013.04.094
528 Shi, C., Day, R.L., 2000a. Pozzolanic reaction in the presence of chemical activators Part
529 I. Reaction kinetics, Cement and Concrete Research 30(1), 51-58. DOI:
530 10.1016/S0008-8846(99)00205-7.
531 Shi, C., Day, R.L., 2000b. Pozzolanic reaction in the presence of chemical activators Part
532 II. Reaction products and mechanism, Cement and Concrete Research 30 (4), 607-
533 613. DOI: 10.1016/S0008-8846(00)00214-3.
534 Tian, S., Jiang, P., Ning, P., Su, Y., 2009. Enhanced adsorption removal of phosphate from
535 water by mixed lanthanum/aluminum pillared montmorillonite, Chemical
536 Engineering Journal, 151(1-3), 141-148. DOI: 10.1016/j.cej.2009.02.006
537 Wang, D., Li, X., Yang, Q., Zheng, W., Wu, Y., Zeng, T., Zeng, G. 2012. Improved
538 biological phosphorus removal performance driven by the aerobic/extended-idle
539 regime with propionate as the sole carbon source, Water Research, 46(12), 3868-3878.
540 DOI: oi.org/10.1016/j.watres.2012.04.036

541 Wang, Z., Shen, D., Shen, F., & Li, T., 2016. Phosphate adsorption on lanthanum loaded
542 biochar. Chemosphere, 150, 1-7. DOI 10.1016/j.chemosphere.2016.02.004
543 Xie, J., Wang, Z., Lu, S., Wu, D., Zhang, Z., Kong, H., 2014. Removal and recovery of
544 phosphate from water by lanthanum hydroxide materials, Chemical Engineering
545 Journal, 254, 163-170. DOI: 10.1016/j.cej.2014.05.113
546 Yanata, S. Nomakuchi, T., Ishibashi, K., 2015. Plant factory engineering strategy of
547 Japanese manufacturer and agri-business innovation, Journal of Agricultural
548 Chemistry and Environment, 4(2), 15. DOI: 10.4236/jacen.2015.42B003
549 Yang, S., Jin, P., Wang, X., Zhang, Q., Chen, X., 2016. Phosphate recovery through
550 adsorption assisted precipitation using novel precipitation material developed from
551 building waste: behavior and mechanism, Chemical Engineering Journal, 292, 246-
552 254. DOI: 10.1016/j.cej.2016.02.006
553 Yao, Z. T., Ji, X. S., Sarker, P. K., Tang, J. H., Ge, L. Q., Xia, M. S., Xi, Y. Q., 2015. A
554 comprehensive review on the applications of coal fly ash, Earth-Science Reviews,
555 141, 105-121. DOI: 10.1016/j.earscirev.2014.11.016
556 Zhang, J., Shen, Z., Shan, W., Chen, Z., Mei, Z., Lei, Y., Wang, W., 2010. Adsorption
557 behavior of phosphate on Lanthanum (III) doped mesoporous silicates material,
558 Journal of Environmental Sciences, 22(4), 507-511. DOI: 10.1016/S1001-

559 0742(09)60141-8

560 Zhang, L., Zhou, Q., Liu, J., Chang, N., Wan, L., & Chen, J. , 2012. Phosphate adsorption

561 on lanthanum hydroxide-doped activated carbon fiber, Chemical Engineering Journal,

562 185-186, 160-167. DOI: 10.1016/j.cej.2012.01.066

563

564

Graphical abstract

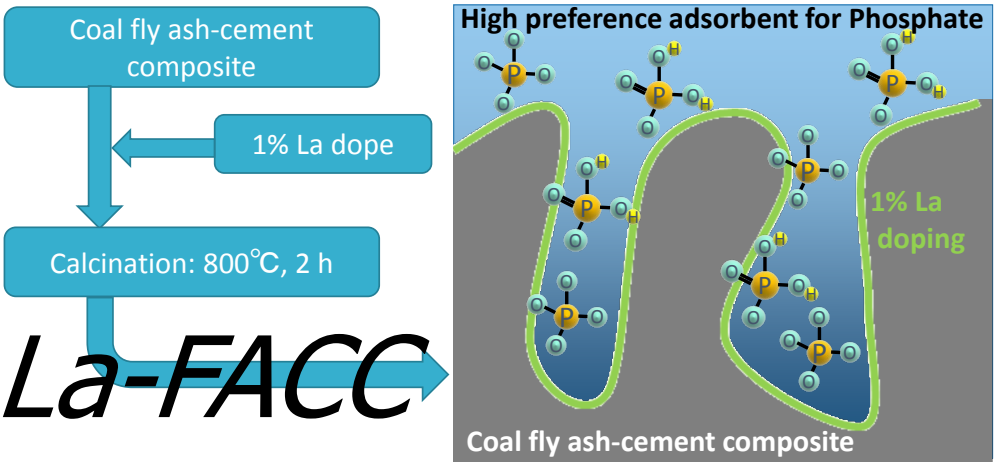

Figures

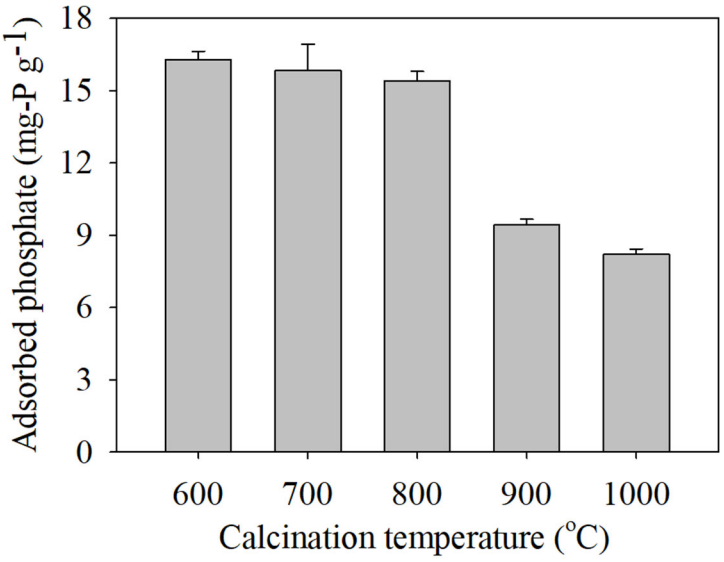


**Fig. 1 Effect of calcination temperature on adsorption phosphate onto the La-FACC.**

Impregnation percentage of La: 4%; Initial phosphate concentration: 100 mg-P $L^{-1}$; La-FACC dosage: 5 g $L^{-1}$; Temperature: 25 ºC; Agitation rate: 100 rpm; Contact time: 168 h; pH at equilibrium: 7.8–8.2.

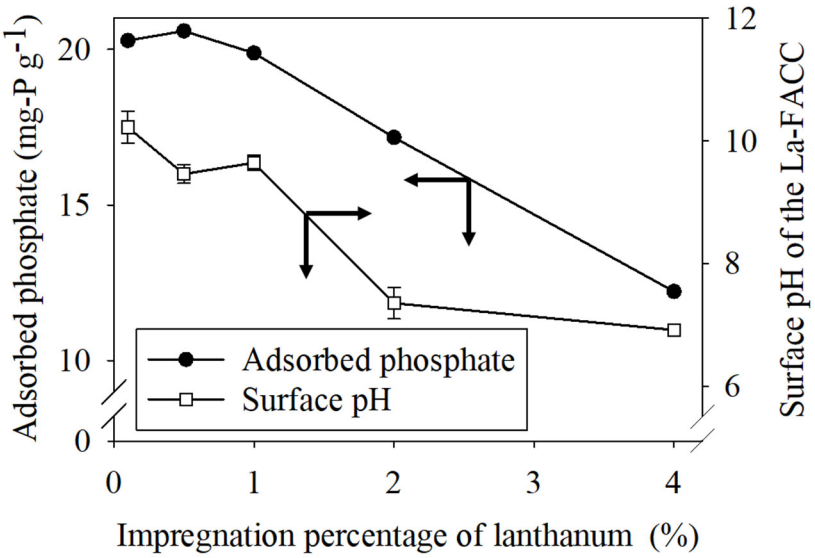


**Fig. 2 Effect of impregnation percentage of La on adsorption capacity of phosphate onto the La-FACC (●) and the surface pH of the La-FACC (□).**

Initial phosphate concentration: 100 mg-P $L^{-1}$; La-FACC dosage: 5 g $L^{-1}$; Temperature: 25 ºC; Agitation rate: 100 rpm; Contact time: 168 h; pH at equilibrium: 7.9–8.3

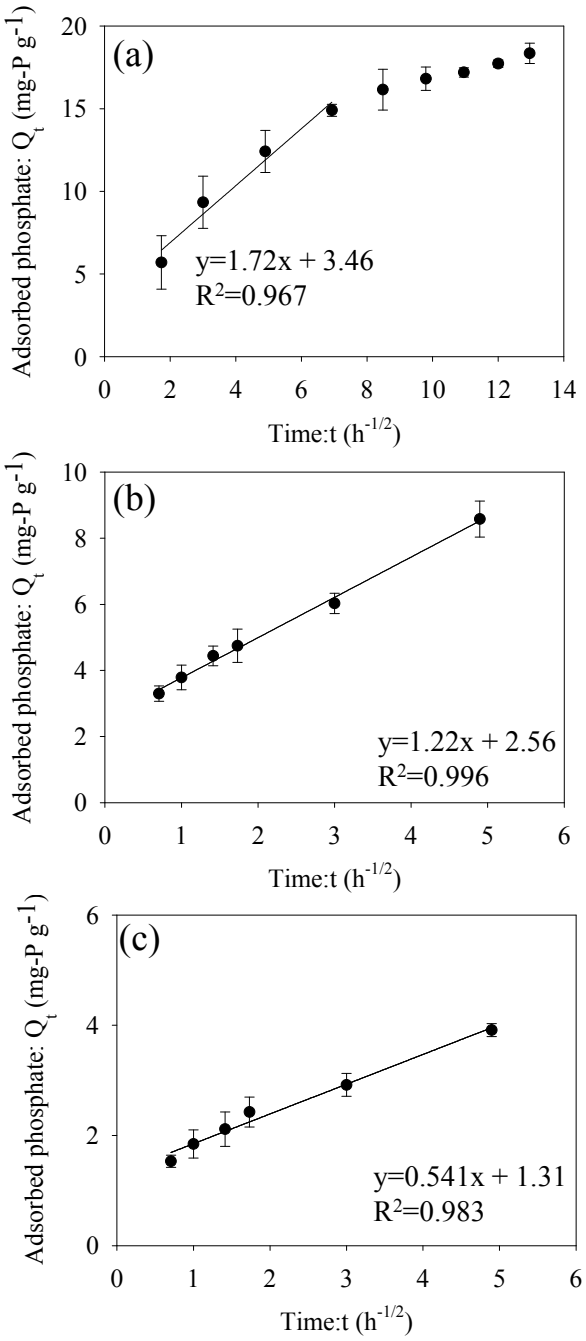


**Fig. 3 Intra-particle diffusion mode for phosphate onto the La-FACC.**

Impregnation percentage of La: 1%; Initial phosphate concentration: (a) 100 mg-P $L^{-1}$; (b) 25 mg-P $L^{-1}$; (c) 10 mg-P $L^{-1}$; La-FACC dosage: 1 g $L^{-1}$; Temperature: 25 ºC; Agitation rate: 100 rpm; pH range: 7.8–8.8

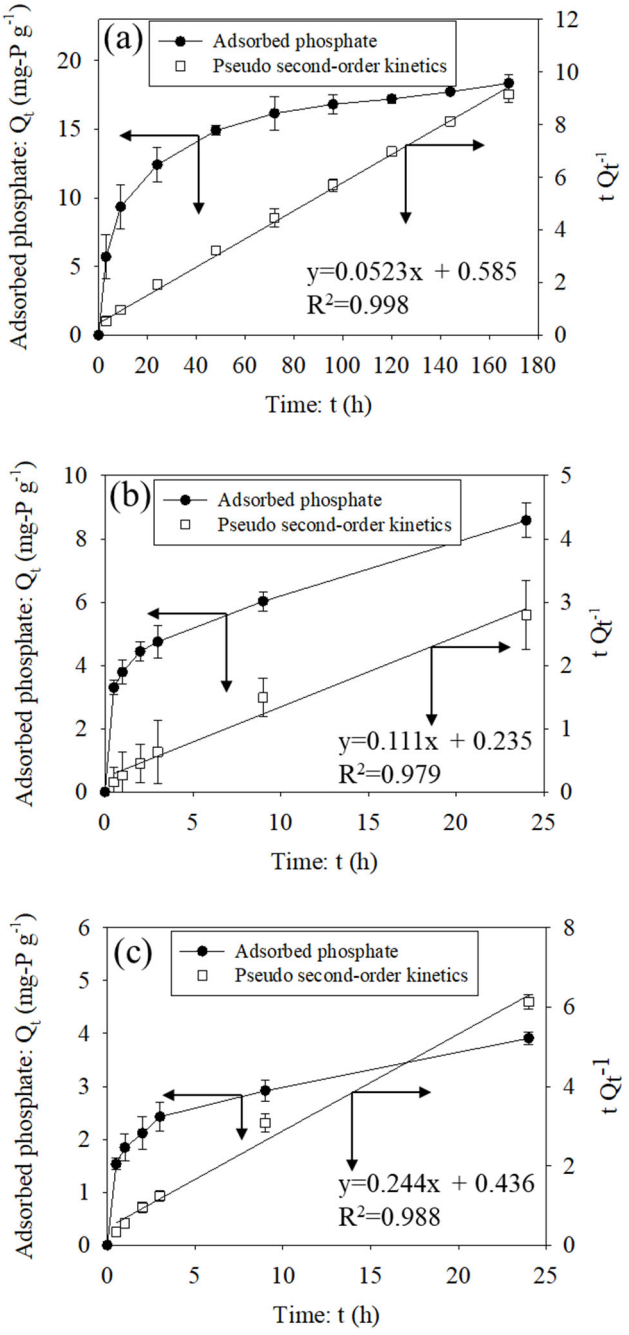


**Fig. 4 Adsorption kinetics and pseudo second-order kinetic model for phosphate onto the La-FACC.**

Adsorbed phosphate (●); Pseudo second-order kinetics (□)

Impregnation percentage of La: 1%; Initial phosphate concentration: (a) 100 mg-P $L^{-1}$; (b) 25 mg-P $L^{-1}$; (c) 10 mg-P $L^{-1}$; La-FACC dosage: 1 g $L^{-1}$; Temperature: 25 ºC; Agitation rate: 100 rpm; pH range: 7.8–8.8

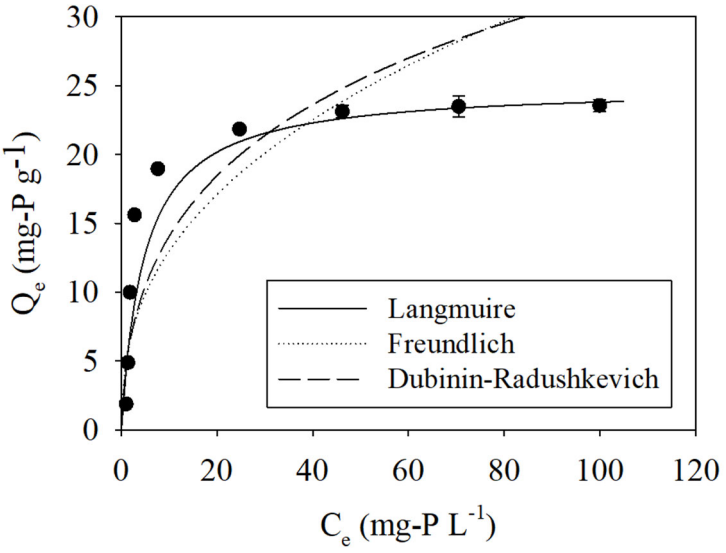


**Fig. 5 Adsorption isotherm for phosphate onto the La-FACC and curved fitting using three adsorption models.**

Impregnation percentage of La: 1%; Initial phosphate concentration: 10–200 mg-P $L^{-1}$; La-FACC dosage: 5 g $L^{-1}$; Temperature: 25 ºC; Agitation rate: 100 rpm; Contact time: 168 h; pH at equilibrium: 8.1–9.1

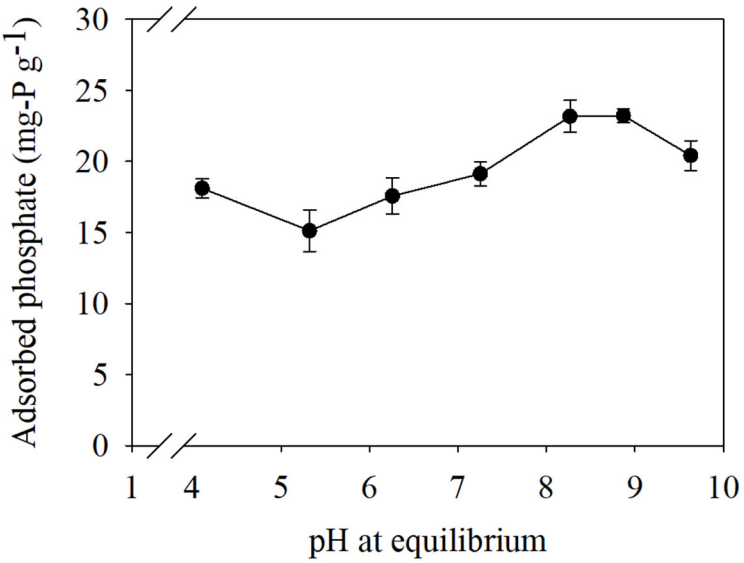


**Fig. 6 Effect of solution pH at equilibrium on adsorption of phosphate onto the La-FACC.**

Impregnation percentage of La: 1%; Initial phosphate concentration: 200 mg-P $L^{-1}$; La-FACC dosage: 5 g $L^{-1}$; Temperature: 25 ºC; Agitation rate: 100 rpm; Contact time: 168 h

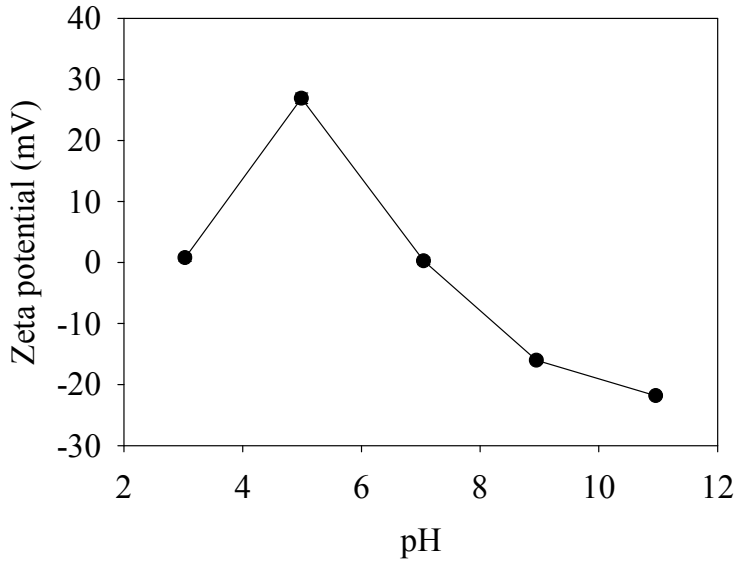


**Fig. 7 The zeta potential of the La-FACC as a function of pH.**

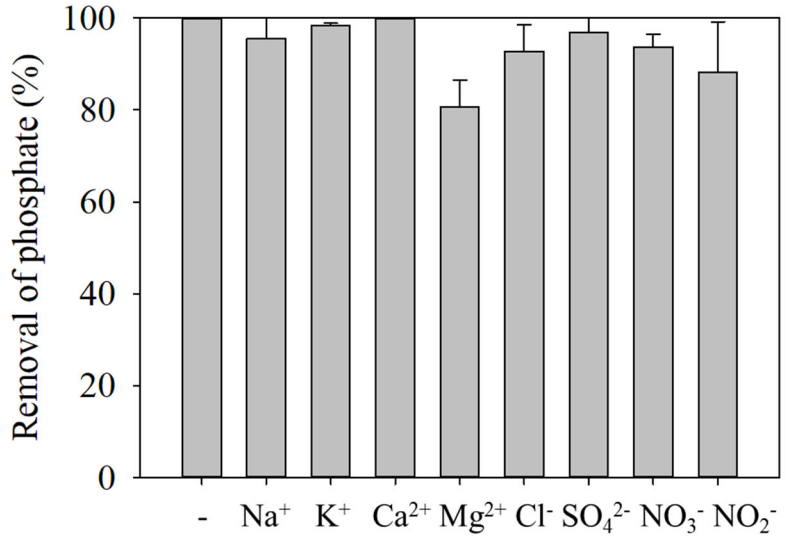


**Fig. 8 Effect of coexisting ions on adsorption of phosphate onto the La-FACC.**

- without any coexisting ions; Impregnation percentage of La: 1%; Initial phosphate concentration: 100 mg-P $L^{-1}$; Coexisting ion concentration: 100 mg-P $L^{-1}$; La-FACC dosage: 5 g $L^{-1}$; Temperature: 25 ºC; Agitation rate: 100 rpm; Contact time: 168 h

Tables

Table 1 Chemical composition of the optimized La-FACC (wt.%)

| | | | |
|---|---|---|---|
| Mg | 0.661 | Mn | 0.049 |
| Al | 7.37 | Fe | 1.71 |
| Si | 24.1 | Cu | 0.0134 |
| P | 0.0958 | Zn | 0.0108 |
| S | 0.576 | Sr | 0.064 |
| Cl | 0.486 | Y | 0.006 |
| K | 0.682 | Zr | 0.0366 |
| Ca | 12.3 | La | 0.984 |
| Ti | 0.465 | | |

Table 2 Parameters for adsorption of phosphate onto the La-FACC obtained by the three kinetic models

| | Pseudo first-order kinetic model | | | Pseudo second-order kinetic model | | | Intra particle diffusion model | | |
|---|---|---|---|---|---|---|---|---|---|
| Initial concentration (mg-P $L^{-1}$) | 100 | 25 | 10 | 100 | 25 | 10 | 100 | 25 | 10 |
| Coefficient of determination ($R^2$) | 0.965 | 0.751 | 0.766 | 0.998 | 0.979 | 0.989 | 0.967* | 0.996 | 0.983 |
| p-value | <0.01 | <0.05 | <0.05 | <0.01 | <0.01 | <0.01 | <0.05* | <0.01 | <0.01 |
| $Q_{e,\,cal}$ | 12.2 | 5.9 | 2.6 | 19.1 | 9.0 | 4.1 | - | - | - |
| $Q_{e,\,obs}$ | 18.4 | 8.6 | 3.9 | 18.4 | 8.6 | 3.9 | - | - | - |
| Deviation of $Q_e$ (%) | 50.9 | 44.3 | 48.2 | -4.0 | -4.8 | -4.4 | - | - | - |
| $k_1$ ($h^{-1}$) | 0.0212 | 0.104 | 0.121 | - | - | - | - | - | - |
| $k_2$ (g $mg^{-1}$ $h^{-1}$) | - | - | - | 0.00467 | 0.0282 | 0.255 | - | - | - |
| $k_i$ (mg $g^{-1}$ $h^{-1/2}$) | - | - | - | - | - | - | 1.72* | 1.22 | 0.54 |

*: $h^{-1/2}$<7

Table 3 Adsorption isotherm for phosphate onto the La-FACC

| | Langmuir | Freundlich | Dubinin–Radushkevich |
|---|---|---|---|
| Coefficient of determination ($R^2$) | 0.992 | 0.657 | 0.703 |
| p-value | <0.01 | <0.01 | <0.01 |
| RMSE | 2.80 | 5.28 | 11.9 |

Supporting materials

# Adsorption of phosphate onto lanthanum doped coal fly ash - blast furnace cement composite

Satoshi ASAOKA[a]*, Kohei KAWAKAMI[b], Hiroyuki SAITO[c],
Tsuyoshi ICHINARI[c], Hideaki NOHARA[d], Takahito OIKAWA[d]

a Research Center for Inland Seas, Kobe University
5-1-1 Fukaeminami, Higashinada, Kobe, Hyogo, 658-0022 JAPAN
(Present address) Graduate School of Integrated Sciences for Life, Hiroshima University
1-4-4 Kagamiyama, Higashi-Hiroshima, Hiroshima, 739-8528 JAPAN
b Graduate school of Maritime Sciences, Kobe University
5-1-1 Fukaeminami, Higashinada, Kobe, Hyogo, 658-0022 JAPAN
c FujiClean Co., LTD.
33 Yamahana, Yamayashiki, Chiryu, Aichi, 472-0022 JAPAN)
d The Chugoku Electric Power Co., INC.
3-9-1, Kagamiyama, Higashi-Hiroshima, Hirosima, 739-0046 JAPAN
*Corresponding author:
Tel: +81-82-424-7945, E-mail: stasaoka@hiroshima-u.ac.jp
Address: Graduate School of Integrated Sciences for Life, Hiroshima University
1-4-4 Kagamiyama, Higashi-Hiroshima, Hiroshima, 739-8528 JAPAN

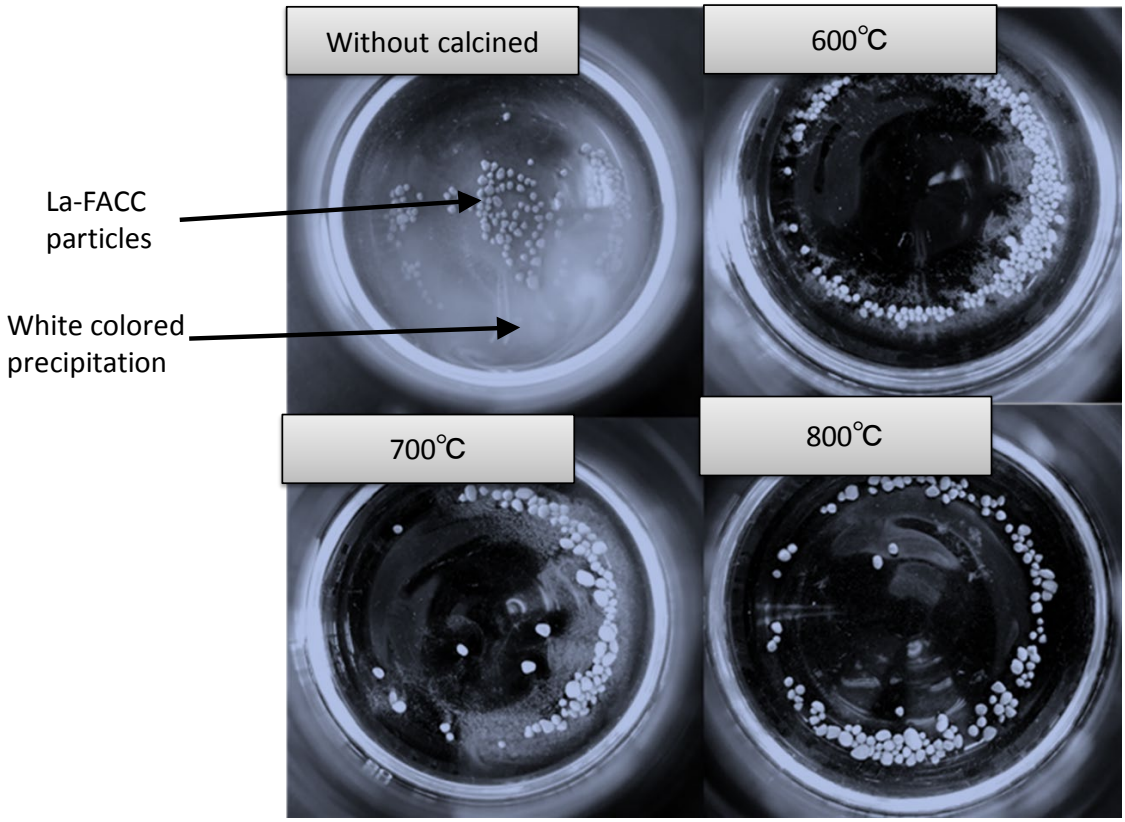


**Fig. S1 Photo of the La-FACC particles (Impregnation percentage of La: 4%) and white colored precipitation**

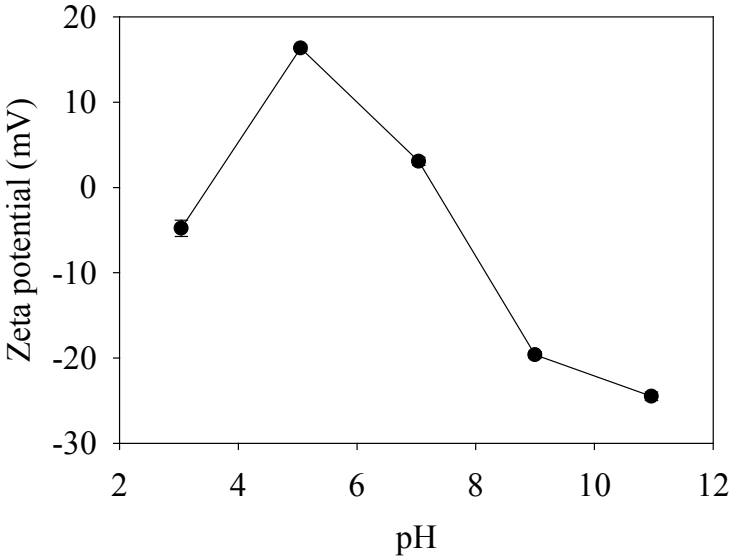


**Fig. S2 The zeta potential of the FACC as a function of pH.**

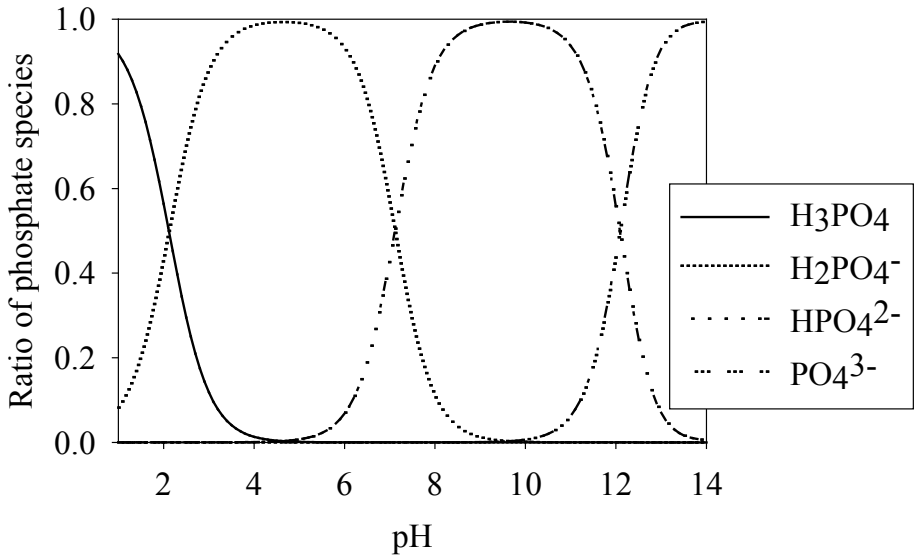


**Fig. S3 Phosphate ion species as a faction of pH**

Phosphate concentration: 100 mg-P $L^{-1;}$ Temperature:25°C